Astron. & Astrophys. 25, 35–40 (1973)

Evolution of Massive Population II Stars

Virginia Trimble*
University of California, Irvine

B. Paczyński
Institute of Astronomy, Warsaw

Barbara A. Zimmerman
California Institute of Technology

Received December 11, 1972

Summary. Evolutionary tracks are presented for 2, 3, 10, 12, and 30 $M_\odot$ stars having $X=0.7$ and $Z=0.001$. Both the main sequence and the Hayashi limit are bluer than for metal-rich stars, and the main sequence models have higher luminosities, central temperatures and densities, and smaller radii. The higher luminosity shortens the time scales of the evolution for a given mass. Helium burning occurs close to the main sequence for the 10, 12, and 30 $M_\odot$ models, rather than in the red giant phase. These differences can be understood qualitatively. The main sequence convective cores, and thus the helium cores formed, are larger than for corresponding higher Z models. Metal-poor stars are therefore capable of contributing a larger amount of helium to the galaxy than metal-rich stars.

Key words: metal-poor stars – Population II stars – helium production

I. Motivation

Apart from the work of Ezer and Cameron (1971) on stars with $Z=0$, and some main sequence models, published calculations for metal-poor stars are available only for masses $\lesssim 1\,M_\odot$. Lack of knowledge of the evolutionary behavior of massive, low metal stars is one of the more serious problems in any attempt to study the evolution of galaxies (Tinsley, 1972). Our understanding of the appearance of galaxies at large distances (i.e. in the past) and of the process of helium and metal enrichment in our own and other galaxies is particularly affected. It was, therefore, decided to evolve a series of stellar models having $X=0.7$ and $Z=0.001$ from the main sequence as far as one hour of computing time on the California Institute of Technology IBM 360/75 would carry them.

II. Computational Details

The stellar evolution program used was that described by Paczyński (1969, 1970). A mixing length of one pressure scale height was adopted in all stellar envelopes. Models with masses, of 2, 3, 10, and 30 $M_\odot$ were chosen initially as providing sufficient coverage of the HR diagram to allow interpolations to be made for other masses. A 12 $M_\odot$ model was added later.
All the evolutionary tracks were terminated by problems irrelevant to astrophysics. The 2 $M_\odot$ track was carried to the point where the hydrogen burning shell was sufficiently thin that the program was no longer very efficient. The 3 and 10 $M_\odot$ tracks were stopped at the onset of helium burning, and the 30 $M_\odot$ track at the onset of carbon burning, when the time step between models was too large to handle the rapidly changing structure of the stars. The 12 $M_\odot$ model exhausted the computing time available for the project.

III. The Evolutionary Tracks

The behavior of the models is summarized in Figs. 1 and 2 and Table 1. Figure 1 represents the evolution of the surfaces of the models in the luminosity-temperature plane, and Fig. 2 the evolution of their centers in the temperature-density plane. Heavy lines indicate the regions where the stars spend most of their time. These are the phases of core hydrogen burning and core helium burning. The tracks can be conveniently com-

* Alfred P. Sloan Foundation Research Fellow.

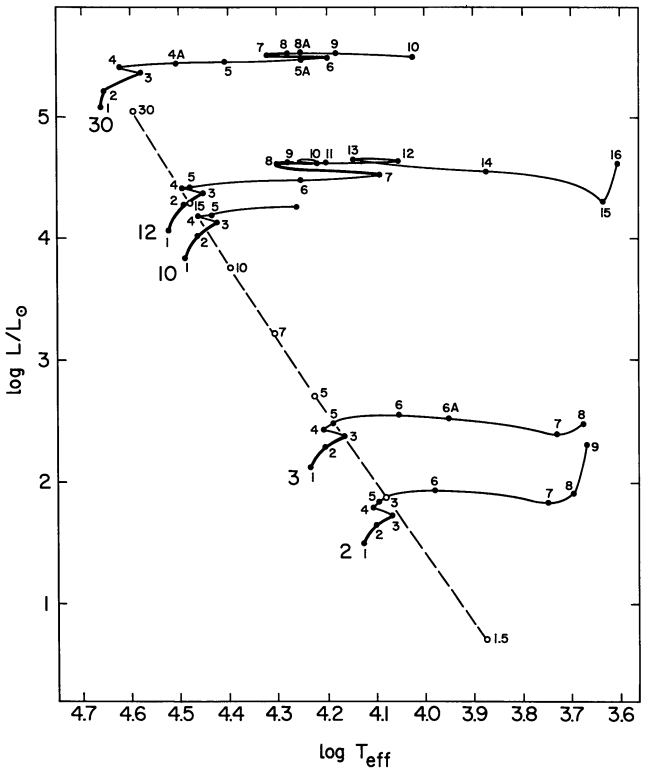

Fig. 1. Evolutionary tracks of $X=0.7$, $Z=0.001$ stars in the luminosity-temperature plane (HR diagram). Heavy parts of the tracks are the phases of core hydrogen and helium burning, where the stars spend most of their time. Numbered points are the models whose properties are shown in Tables 1 and 2. The main sequence is shown for $Z=0.03$ stars (dashed line). Metal-rich main sequence models are shown as open circles. Masses are in solar masses

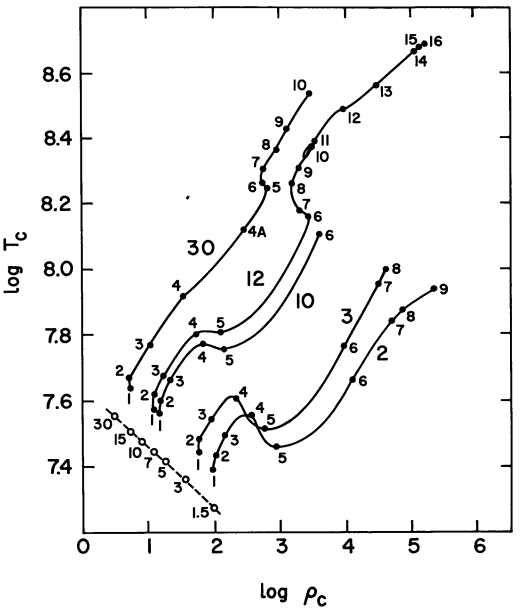

Fig. 2. Evolution of the centers of $X=0.7$, $Z=0.001$ stars in the temperature-density plane. Numbered points are the models whose properties are shown in Tables 1 and 2. Main sequence models with $X=0.7$, $Z=0.03$ are shown as open circles. Masses are in solar masses

pared with those for $X=0.7$, $Z=0.03$ stars given by Paczyński (1970), which were prepared using the same evolutionary code. Table 1 includes information on the time scales of the evolution and the internal structure of the models at various stages.

Table 1. Properties of stellar models with $X=0.7, Z=0.001$ at points marked in Figs. 1 and 2

Point	Time[a]	$\log L/L_\odot$[b]	$\log T_{eff}$[c]	$\log T_c$[d]	$\log \varrho_c$[e]	M_{conv} core[f]	M_{conv} env[g]	X_c or $M(X=0)$[h]	Y_c or $M(Y=0)$[i]	C_c[j]
30 solar masses										
1	0.0	5.086	4.6608	7.6397	0.7243	17.352	–	0.70000	0.29900	0.0
2	1.7718(6)	5.193	4.6505	7.6578	0.7217	14.162	–	0.52030	0.42870	0.0
3	3.9979(6)	5.356	4.5821	7.7450	0.9579	8.833	–	0.03290	0.96610	0.0
4	4.0809(6)	5.393	4.6223	7.9129	1.5192	2.473	–	(4.341)	0.99900	0.0
4A	4.0926(6)	5.472	4.5050	8.1222	2.4506	0.030	–	(6.701)	0.99899	0.0
5	4.0987(6)	5.447	4.4077	8.2501	2.7910	2.725	–	(7.609)	0.99334	0.00564
6	4.1319(6)	5.476	4.1961	8.2628	2.7291	5.488	–	(8.828)	0.92569	0.07226
7	4.3422(6)	5.493	4.3196	8.3107	2.7696	7.381	–	(10.757)	0.43475	0.50967
8	4.4422(6)	5.470	4.2810	8.3712	2.9510	7.759	–	(11.279)	0.11021	0.64176
9	4.4905(6)	5.501	4.2011	8.4357	3.1249	7.786	–	(11.541)	0.01374	0.48568
10	4.5009(6)	5.478	4.0225	8.5379	3.4440	6.782	–	(11.651)	0.00007	0.44078
12 solar masses										
1	0.0	4.068	4.5194	7.5775	1.0742	4.661	–	0.70000	0.29900	0.0
2	7.4172(6)	4.272	4.4879	7.6180	1.0958	2.980	–	0.35299	0.64601	0.0
3	9.9825(6)	4.369	4.4540	7.6731	1.2310	2.132	–	0.05769	0.94131	0.0
4	1.0308(7)	4.412	4.4910	7.8076	1.7587	0.534	–	0.00007	0.99893	0.0
5	1.0315(7)	4.403	4.4780	7.8073	2.0193	0.012	–	(0.878)	0.99900	0.0
6	1.0391(7)	4.479	4.2494	8.1642	3.4302	0.249	–	(1.990)	0.99563	0.00336
7	1.0435(7)	4.522	4.0903	8.1811	3.2964	0.770	–	(2.179)	0.97557	0.02337
8	1.1497(7)	4.601	4.2978	8.2660	3.1947	1.614	–	(3.278)	0.30398	0.61461
9	1.1696(7)	4.613	4.2818	8.3086	3.2878	1.739	–	(3.394)	0.11774	0.68611
10	1.1780(7)	4.618	4.2169	8.3384	3.3616	1.864	–	(3.494)	0.01251	0.60064

Table 1 (continued)

Point	Time[a])	$\log L/L_\odot$[b])	$\log T_{\rm eff}$[c])	$\log T_c$[d])	$\log \varrho_c$[e])	$M_{\rm conv}$[g]) core	$M_{\rm conv}$[g]) env	X_c or $M(X=0)$[h])	Y_c or $M(Y=0)$[i])	C_c[j])
11	1.1861(7)	4.620	4.2042	8.3906	3.5290	1.887	–	(3.554)	0.00935	0.46325
12	1.1887(7)	4.621	4.0579	8.4903	3.9898	0.003	–	(3.575)	0.0	0.43550
13	1.1912(7)	4.623	4.1391	8.5674	4.4932	0.003	–	(3.575)	(1.161)	0.43550
14	1.1934(7)	4.547	3.8707	8.6646	5.0126	0.002	–	(3.575)	(1.414)	0.43550
15	1.1936(7)	4.305	3.6316	8.6827	5.1164	0.002	10.284	(3.575)	(1.470)	0.43550
16	1.1937(7)	4.601	3.6024	8.6879	5.1482	0.002	4.548	(3.575)	(1.470)	0.43550
10 solar masses										
1	0.0	3.840	4.4861	7.5636	1.1525	3.599	–	0.70000	0.29900	0.0
2	8.7525(6)	4.021	4.4665	7.5922	1.1644	2.503	–	0.39935	0.59965	0.0
3	1.2836(7)	4.130	4.4215	7.6610	1.3191	1.534	–	0.70000	0.29900	0.0
4	1.3214(7)	4.176	4.4575	7.7739	1.7695	0.544	–	0.00027	0.99873	0.0
5	1.3231(7)	4.176	4.4376	7.7591	2.1612	0.010	–	(0.567)	0.99900	0.0
6	1.3363(7)	4.243	4.2226	8.1109	3.5929	0.011	–	(1.467)	0.99750	0.00150
3 solar masses										
1	0.0	2.137	4.2275	7.4476	1.7698	0.725	–	0.70000	0.29900	0.0
2	9.0079(7)	2.294	4.1995	7.4836	1.7924	0.440	–	0.45264	0.54636	0.0
3	1.3012(8)	2.380	4.1665	7.5452	1.9497	0.251	–	0.05332	0.94568	0.0
4	1.3362(8)	2.430	4.2002	7.6092	2.3147	0.044	–	0.00094	0.99805	0.0
5	1.3634(8)	2.468	4.1869	7.5161	2.8127	0.003	–	(0.098)	0.99900	0.0
6	1.4419(8)	2.547	4.0533	7.7687	3.9806	0.003	–	(0.320)	0.99900	0.0
7	1.4562(8)	2.389	3.7301	7.9626	4.5135	0.003	2.478	(0.395)	0.99899	0.00001
8	1.4592(8)	2.468	3.6746	8.0029	4.6009	0.002	1.583	(0.402)	0.99843	0.00057
2 solar masses										
1	0.0	1.497	4.1219	7.3955	1.9748	0.383	–	0.70000	0.29900	0.0
2	2.4275(8)	1.646	4.0989	7.4383	2.0241	0.263	–	0.40644	0.59256	0.0
3	3.5338(8)	1.724	4.0661	7.4921	2.1559	0.153	–	0.07155	0.92745	0.0
4	3.6623(8)	1.786	4.1018	7.5565	2.5390	0.023	–	0.00110	0.99790	0.0
5	3.7767(8)	1.862	4.0927	7.4646	2.9543	0.002	–	(0.066)	0.99900	0.0
6	4.0888(8)	1.928	3.9788	7.6634	4.0989	0.002	–	(0.211)	0.99900	0.0
7	4.1626(8)	1.824	3.7449	7.8424	4.6860	0.002	1.584	(0.276)	0.99900	0.0
8	4.1932(8)	1.894	3.7177	7.8771	4.8578	0.002	1.028	(0.290)	0.99900	0.0
9	4.3144(8)	2.297	3.6656	7.9377	5.2905	0.0	0.415	(0.333)	0.99811	0.00088

[a]) Time in years from main sequence model. Exponent in parentheses.
[b]) log of luminosity in solar units.
[c]) log of effective temperature in °K.
[d]) log of central temperature in °K.
[e]) log of central density in g cm^{-3}.
[f]) Outer edge of convective core in $M_\odot$.
[g]) Inner edge of convective envelope in $M_\odot$.
[h]) Central hydrogen abundance or, in parentheses, outer edge of core in which hydrogen has been exhausted, in $M_\odot$.
[i]) Central helium abundance or, in parentheses, outer edge of core in which helium has been exhausted, in $M_\odot$.
[j]) Central carbon abundance.

IV. Discussion and Comparison with Higher Z Models

Significant differences between these stars and ones with higher metal content occur both in the main sequence models and in the evolutionary tracks. The $Z=0.001$ stars have higher luminosities, effective temperatures, central densities and temperatures, and larger convective cores on the main sequence than $Z=0.03$ stars calculated with the same program. In addition, the evolutionary time scales are shorter, helium ignition occurs nearer the main sequence, the Hayashi limit is bluer, and more helium is produced in the low metal models.

Figures 1 and 2 show the zero-age main sequences for both low metal and high metal abundance stars in the luminosity-effective temperature and central temperature-central density planes. Data for the models with $X=0.7$ and $Z=0.03$ are taken from Paczyński (1970) and Ziołkowski (1972; for the $30\,M_\odot$ model). The differences are a straightforward result of the different metal abundances. Energy generation in the CNO cycle is, of course, proportional to metal abundance. Thus a lower Z star requires higher values of central density and temperature to maintain thermal equilibrium. The greater degree of central compactness then decreases the star's radius and increases its effective temperature. In addition, the Kramer's part of the opacity in the stellar envelope depends linearly on Z. Thus the lower Z models should have higher

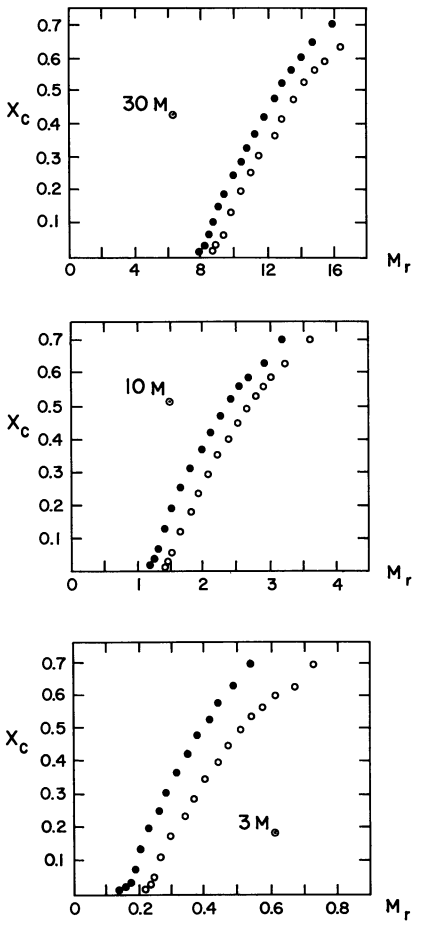

Fig. 3. Variation of convective core masses as a function of central hydrogen content, X_c for 30, 10, and 3 $M_\odot$ stars. The shape of the hydrogen profile, $X(M_r)$, at the time of central hydrogen exhaustion is the same. Models with $Z=0.03$ are shown as dots; models with $Z=0.001$ as open circles. All stars were followed with the same evolutionary program, neglecting semiconvection. Data for the 30 $M_\odot$, $Z=0.03$ star is taken from Ziołkowski (1972)

luminosities (cf. Schwarzschild, 1958), the difference being greatest for low mass models, where bound-bound and bound-free transitions in metals dominate electron scattering as the source of opacity.

Figure 3 shows the changing size of the convective core in 3, 10, and 30 $M_\odot$ models as the central hydrogen abundance drops from 0.7 to 0.0 for two metal abundances. The $Z=0.03$ models are those discussed by Paczyński (1970) and Ziołkowski (1972). The cores are larger at all phases for the lower metal abundance. In particular, a low-metal main sequence model has about the same amount of mass in its convective core as a high-metal main sequence model with the same luminosity (and somewhat higher total mass).

This seems at least not implausible if one writes the criterion for stability against convection in the form

$$\frac{T^3 M_r}{\varkappa \varrho L_r} > \frac{3K}{16\pi acG\mu H}\left(\frac{\gamma}{\gamma-1}\right) \approx \text{const.}$$

Table 2. Time in years elapsed from main sequence to points in evolutionary tracks shown in Fig. 1. Exponents given in parenthese

Point in Fig. 1	Time since M.S. $X=0.7, Z=0.001$	Time since M.S. $X=0.708, Z=0.02$ [a])	Ratio $\frac{Z=0.02}{Z=0.001}$
3 $M_\odot$			
1	0.0	2.510(6)	—
3	1.3012(8)	2.273(8)	1.74
4	1.3362(8)	2.394(8)	1.78
6 A	1.4480(8)	2.478(8)	1.72
7	1.4562(8)	2.488(8)	1.78

Point in Fig. 1	Time since M.S. $X=0.7, Z=0.001$	Time since M.S. $X=0.7, Z=0.03$ [b])	Ratio $\frac{Z=0.03}{Z=0.001}$
30 $M_\odot$			
1	0.0	2.(4)	—
3	3.9979(6)	4.82(6)	1.21
4	4.0809(6)	4.91(6)	1.20
5 A	4.1130(6)	4.92(6)	1.19
6	4.1319(6)	4.93(6)	1.19
8 A	4.4580(6)	5.45(6)	1.22

[a]) Data from model by Iben quoted in Cox and Giuli (1968).
[b]) Data from model by Stothers quoted in Cox and Giuli (1968).

where T, ϱ, and $\varkappa$ are the temperature, density, and opacity at a given layer in the star; M_r and L_r are the mass and luminosity interior to that layer; μ and γ are the mean molecular weight and ratio of specific heats of the gas; and the rest are physical constants. The opacity is largely due to electron scattering in the deep interior and is thus independent of metal abundance, as is the mean molecular weight. Hence, other things being equal, a model which has more luminosity interior to a given layer is more likely to be convective there. The low Z models also have higher interior densities and temperatures, the former tending to produce convection and the latter to inhibit it; but the effect of the luminosity appears to dominate.

The larger luminosity of the low metal models is also directly correlated with their evolutionary time scales, the stars using up more rapidly the stores of energy available to them. Table 2 is a comparison of the times taken for high and low Z models of 3 and 30 $M_\odot$ to evolve from the main sequence to points shown in Figs. 1 and 2. The data for the metal rich stars is from work by Iben and Stothers, as summarized by Cox and Giuli (1968). The metal-poor 3 $M_\odot$ star evolves, on the average, about 1.75 times as fast as the metal-rich one, and its main sequence model is 1.74 times as luminous. The metal-poor 30 $M_\odot$ star (for which the decreased opacity is less important) evolves about 1.2 times as fast as the metal-rich one, and its main sequence model is 1.16 times as luminous.

The tracks of the 2, 3, and 12 $M_\odot$ models begin turning toward higher luminosity in the red giant region at effective temperatures which are 10–15% higher than the turn-up points for the $Z=0.03$ stars studied by Paczyński (1970).

Core helium burning occurs systematically earlier on the evolutionary tracks of the lower metal abundance stars: in the blue supergiant region for the 12 and 30 $M_\odot$ models, and immediately after reaching the red giant region for the 3 $M_\odot$ model. Effects of this type were predicted by Arnett (private communication, 1970) and can be understood qualitatively. All of the low Z stars have higher central densities and temperatures and smaller radii on the main sequence, and form larger helium cores, than the corresponding high Z stars. Since energy generation by the triple alpha process depends only on density and temperature (in a core which is nearly pure helium anyway) this means that, on the one hand, the cores of the low Z stars need to do less contracting to reach helium burning conditions, while, on the other hand, more energy has to be put into their envelopes, whose gravitational binding is greater, to expand them to red giant configurations. This is consistent with the result of Trimble and Paczyński (1972), who found that lowering the metal abundance makes it more difficult to form helium red giants.

In the case of 3 $M_\odot$ models, stars of both compositions had helium core masses below the effective Schönberg-Chandrasekhar (1942) limit[1]) at the time of central hydrogen exhaustion, and thus burned hydrogen in a thick shell for a while, remaining near the main sequence. But when they reached the red giant region, the low metal star had a significantly larger helium core (0.39 $M_\odot$ compared to 0.28 $M_\odot$ for $Z=0.03$) and thus was able to ignite helium almost immediately. The higher Z model, on the other hand, burned hydrogen in a thin shell after reaching the red giant region, and helium was ignited when the core mass reached about 0.35 $M_\odot$.

The 10, 12, and 30 $M_\odot$ stars had initial core masses above the Schönberg-Chandrasekhar limit at the time of central hydrogen exhaustion, and thus left the main sequence immediately. Their subsequent behavior can be related to the possible locations on the HR diagram of static, helium burning models with $X(M_r)$ profiles like those left after the main sequence phase.

The phenomena have been well-studied in the case of metal-rich, massive stars. Evolutionary tracks by both Chiosi and Summa (1970) and Simpson (1971) show that, if a large amount of convective or semiconvective mixing is allowed, the stars begin burning helium in the blue super giant region, while if no mixing is allowed, the stars move rapidly to the red supergiant region and ignite helium there. Static models of stars with core helium burning have been considered by Lauterborn *et al.* (1971a, b) and by Kozłowski (1971). They find that if semi-convective mixing of matter eliminates or greatly reduces the mass of the region with varying $X(M_r)$ above the hydrogen burning shell, then only a high effective temperature (blue supergiant) static model exists for a given core mass. If, however, the $X(M_r)$ is the one left behind by the shrinking convective core during main sequence hydrogen burning without mixing, then there are two static helium burning models with a given core mass in the blue and red regions of the HR diagram (and a third, unstable, one in between), and the star can jump between them. Thus a high metal evolutionary model with mixing burns helium as a blue supergiant and is associated with a single, blue static model, while an evolutionary model without mixing burns helium as a red supergiant and is associated with two possible static models.

Our evolutionary tracks for low metal stars were calculated without any semiconvective mixing, but the 10, 12, and 30 $M_\odot$ models ignited helium as blue supergiants. They thus mimic high metal, mixed models in this, as well as in the loops in the HR diagram during the phase of core helium burning, and ought, therefore, to be associated with no more than one static model.

The low metal abundance stars contain a larger amount of helium at all post main sequence phases than their high metal analogues. The last 30 $M_\odot$ model shown in Fig. 1 contains 7.48 $M_\odot$ more of carbon and oxygen and 1.58 $M_\odot$ more of helium than did the main sequence configuration (account having been taken of the helium initially present in the core which is destroyed by the triple alpha process). The corresponding numbers for the last 12 $M_\odot$ model shown are 1.90 and 0.56 $M_\odot$. The last models of the 10, 3, and 2 $M_\odot$ tracks contain 1.67, 0.93, and 0.245 $M_\odot$ of additional helium respectively and less than 0.001 $M_\odot$ of additional carbon, since helium burning had not really started. Each generation of high mass, low metal stars early in the history of the galaxy may, therefore, have been capable of increasing Y of the material involved by several percent. Helium enrichment from massive, high Z stars is probably negligible (Tinsley, 1972).

Acknowledgements. We are indebted to Dr. Beatrice M. Tinsley for pointing out the importance of high mass, low metal stars and Dr. J. Ziołkowsky for use of material in advance of publication. The computing was supported by the National Science Foundation, Grant No. GP 31413 to Drs. J. B. Oke and J. E. Gunn at California Institute of Technology. VT gratefully acknowledges the hospitality of the Department of Physics and Astronomy, University of Maryland, where this work was completed.

[1]) The fraction of the mass of a star that can be contained in the isothermal core of an equilibrium model is a decreasing function of the ratio of core mean molecular weight to envelope mean molecular weight. Thus any smoothing of the composition discontinuity across the boundary will increase the Schönberg-Chandrasekhar limit.

References

Chiosi, C., Summa, C. 1970, *Astrophys. Space Sci.* **8**, 478.
Cox, J. P., Giuli, R. T. 1968, Principles of Stellar Evolution, Gordon and Breach, New York, p. 987–988.
Ezer, D., Cameron, A. G. W. 1971, *Astrophys. Space Sci.* **14**, 399.
Kozłowski, M. 1971, *Astrophys. Letters* **9**, 65.
Lauterborn, D., Refsdal, S., Weigert, A. 1971a, *Astron. & Astrophys.* **10**, 97.
Lauterborn, D., Refsdal, S., Roth, M. L. 1971b, *Astron. & Astrophys.* **13**, 119.
Paczyński, B. 1969, *Acta Astron.* **19**, 1.
Paczyński, B. 1970, *Acta Astron.* **20**, 47.
Schönberg, M., Chandrasekhar, S. 1942, *Astrophys. J.* **96**, 161.
Schwarzschild, M. 1958, Structure and Evolution of the Stars, University Press Princeton, equations 15.9 and 15.24, p. 130.
Simpson, E. 1971, *Astrophys. J.* **165**, 295.
Tinsley, B. M. 1972, *Astron. Astrophys.* **20**, 383 and private communication.
Trimble, V., Paczyński, B. 1972, *Astron. & Astrophys.* **22**, 1.
Ziołkowski, J. 1972, *Acta Astron.* **22**, in press.

Virginia Trimble
Department of Physics
University of California
Irvine, California 92664, USA

B. Paczyński
Zaktad Astronomii
Polskiej Akademii Nauk
Al. Ujazdowskie 4
Warszawa, Poland

Barbara A. Zimmerman
Kellogg Laboratory
California Institute of Technology
Pasadena, California 91109, USA